Structured Packing Performance—Experimental Evaluation of Two Predictive Models

James R. Fair,*,† A. Frank Seibert,† M. Behrens,‡ P. P. Saraber,‡ and Z. Olujic‡

Department of Chemical Engineering, The University of Texas at Austin, Austin, Texas 78712, and Laboratory for Process Equipment, Delft University of Technology, 2628 CA Delft, The Netherlands

A comprehensive total reflux distillation study of sheet metal structured packings was carried out with the cyclohexane/*n*-heptane test mixture. The experiments covered a wide range of pressures, two corrugation angles, two surface areas, and two surface designs. Experimental results include pressure drop, capacity, and mass-transfer efficiency. The database generated has been used to evaluate generalized performance models developed independently at The University of Texas Separations Research Program (SRP model)) and at Delft University of Technology (Delft model). This paper reports the experimental results and compares them with predictions from the two models. Deviations of predictions from measurements are discussed in terms of likely contacting mechanisms in the packed bed.

Introduction

Corrugated structured packings are used widely in distillation columns. Early versions were fabricated from metal gauze and had a specific surface area of about 500 m^2/m^3. Later versions were fabricated from the more economical sheet metal and had a specific surface area of about 250 m^2/m^3 and a corrugation angle (with respect to the horizontal) of 45°. This geometry became a rather standard design of several manufacturers/vendors, and most of the reported performance data have been based on tests with the 250 m^2/m^3 surface and 45° angle. More recently, the manufacturers have begun to offer sheet metal packings with various surface areas and a larger corrugation angle to satisfy growing needs for more efficiency or capacity. However, published data on the performance of such structured packings are scarce, and current models for predicting their performance have not been validated adequately. The purpose of this paper is to provide new performance data for sheet metal packings that embody two corrugation angles and different combinations of surface area and surface treatment, to ascertain how well available predictive models fit the data.

A model often used for predicting mass transfer and hydraulic performance of structured packings was developed several years ago at the Separations Research Program (SRP) of The University of Texas at Austin.[1−3] The basis for the model is a modified wetted-wall flow arrangement through the channels of the packing. An alternate model has been developed more recently at the Delft University of Technology[4−6] and is also founded on liquid film flow down inclined corrugated plates and in addition takes into account explicitly several macro geometrical parameters which can affect packing performance. For a thorough evaluation of predictive models, it has been necessary to await experimental work at a semiworks scale using a consistently fabricated set of packings that could provide internally consistent data. And, of course, the data had to be made available to the public if studies could be continued by others.

Recent experiments at the SRP have provided the needed data. To achieve meaningful and consistent comparative results, we felt it necessary to use the packings of a single manufacturer. To this end, the Julius Montz Co., of Hilden, Germany, agreed to furnish a set of packings with two corrugation angles (45° and 60°), two surfaces (shallow embossed, nonperforated and expanded metal, perforated), and two specific surface areas. The characteristics of these packings are shown in Table 1. This unique data set has been used to validate SRP and Delft performance predictive models.[1−6] In the present paper we present comparisons between model and experimental values, shortcomings of the models, and the potential for their improvement.

SRP and Delft Models

A summary of working equations of the SRP and Delft models is given in Tables 2−4. Table 2 shows expressions common to both methods, which include equations for predicting load point as well as the effect of loading on pressure drop. Characteristic expressions for the individual models are given in Tables 3 and 4. One should note that the expression for the hydraulic diameter of a gas flow channel (eq 11) requires liquid film thickness, which is calculated using the appropriate correlation from Table 3 or 4, depending on the method used. The same approach is valid for liquid holdup in eqs 6 and 7, to provide effective gas and liquid velocities, and in eqs 14 and 15 for the heights of mass-transfer units for the gas and liquid phases.

SRP Model. This model (Bravo et al.[1−3]) has been modified recently by Gualito et al.[7] to better represent higher pressure performance. Basically, the SRP model considers the bed as a series of parallel, inclined wetted-wall columns with a characteristic cross section and an equivalent diameter equal to the side dimension of the corrugation. This macroscopic parameter does not account for the effects of proprietary designs of corrugations and surface; such are taken into account by using coefficients regressed from experimental data coupled

* To whom correspondence should be addressed. E-mail: Fair@che.utexas.edu.

† The University of Texas at Austin.

‡ Delft University of Technology.

10.1021/ie990910t CCC: $19.00
Published on Web 05/06/2000

Table 1. Characteristics of the Packings Tested

packing	surface (m^2/m^3) a_p	void fraction (m^3/m^3) ϵ	corrugation angle (deg)	element height h_{pe} (m)	channel dimensions (m) base b	height h	side s	description
B1-250	244	0.980	45	0.194	0.0225	0.0120	0.01645	shallow embossed, unperforated
B1-250.60	245	0.978	60	0.211	0.0223	0.0120	0.01645	shallow embossed, unperforated
B1-400	394	0.960	45	0.197	0.0140	0.0074	0.01033	shallow embossed, unperforated
B1-400.60	390	0.960	60	0.196	0.0143	0.0074	0.01029	shallow embossed, unperforated
BSH-400	378	0.970	45	0.194	0.0151	0.0074	0.01058	expanded metal, perforated
BSH-400.60	382	0.970	60	0.215	0.0148	0.0074	0.01047	expanded metal, perforated

Table 2. Common Equations, SRP, and Delft

required input variables: α, ϵ, h, b, h_{pe}, n_{pe}, ρ_G, ρ_L, μ_G, μ_L, σ, D_G, D_L, λ, and F_G

(A) Packing Geometry and Flow-Related Parameters

height of the packed bed:

$$h_{pb} = n_{pe}h_{pe} \quad (1)$$

installed specific surface area of packing:

$$a_p = 4s/bh \quad (2)$$

corrugation side length:

$$s = \sqrt{(b^2/4) + h^2} \quad (3)$$

superficial gas and liquid velocities:

$$u_{Gs} = F_G/\sqrt{\rho_G} \quad (4)$$

$$u_{Ls} = u_{Gs}(\rho_G/\rho_L) \quad (5)$$

effective gas and liquid velocities

$$u_{Ge} = u_{Gs}/[\epsilon(1 - h_L)\sin\alpha] \quad (6)$$

$$u_{Le} = u_{Ls}/[\epsilon h_L \sin\alpha] \quad (7)$$

for liquid holdup, h_L, different expressions are utilized by SRP and Delft methods.

(B) Pressure Drop

full operating range:

$$\left(\frac{\Delta p}{\Delta z}\right) = \left(\frac{\Delta p}{\Delta z}\right)_{preload} F_{load} \quad (8)$$

pressure drop enhancement factor for the loading region:

$$F_{load} = 3.8\left(\frac{F_G}{F_{G,lp}}\right)^{2/\sin\alpha}\left(\frac{u_{Ls}^2}{\epsilon^2 g d_{hG}}\right)^{0.13} \quad (9)$$

loading point F-factor, i.e., the point of departure from preloading conditions:

$$F_{G,lp} = \left(0.053\epsilon^2 g d_{hG}(\rho_L - \rho_G)\left(\frac{u_{Ls}}{u_{Gs}}\sqrt{\frac{\rho_L}{\rho_G}}\right)^{-0.25}(\sin\alpha)^{1.15}\right)^{0.5} \quad (10)$$

hydraulic diameter of triangular gas flow channel:

$$d_{hG} = \left\{\frac{(bh - 2\delta s)^2}{bh}\right\}/\left\{\left[\left(\frac{bh - 2\delta s}{2h}\right)^2 + \left(\frac{bh - 2\delta s}{b}\right)^2\right]^{0.5} + \frac{bh - 2\delta s}{2h}\right\} \quad (11)$$

(C) Mass-Transfer Efficiency

$$HETP = [(\ln\lambda)/(\lambda - 1)]HTG_{Go} \quad (12)$$

$$HTU_{Go} = HTU_G + \lambda HTU_L \quad (13)$$

$$HTU_G = u_{Gs}/(k_G a_e) \quad (14)$$

$$HTU_L = u_{Ls}/(k_L a_e) \quad (15)$$

stripping factor for total reflux ($L/V = 1$) situation:

$$\lambda = m = \alpha_{lk}/[1 + (\alpha_{lk} - 1)x_{lk}]^2 \quad (16)$$

with a friction factor for dry pressure drop. The effect of liquid flow on pressure drop utilizes liquid holdup as a major variable, directly related to average film thickness and effective surface area. Because the film thickness depends on the effective gravity, the calculation procedure is implicit. A pressure drop of 10.25 mbar/m is generally recommended as a flooding point pressure drop, which in some cases has to be increased to about 20 mbar/m to ensure convergence. The spreading tendency of the liquid is accounted for by the contact angle between the liquid and the particular surface used. Enhancement of the surface by texturing is represented by a correction factor based on laboratory tests. Because an experimental value of the correction factor was not available for the packings used in this study, an assumption/interpolation was made ($F_{se} = 0.35$, see eq 27) on the basis of a comparison of surface characteristics of packings of this study and other packings from the SRP database.

Delft Model. This model[4−6] utilizes zig-zag triangular flow channels with a corresponding hydraulic diameter at crossings of corrugations. The open side at a crossing of corrugations is an interface between two gas flows and is responsible for a considerable loss of energy. Friction at the gas−liquid interface is a much smaller contributor to pressure drop. Sharp bends between elements also contribute significantly to pressure drop. Importantly, the model is based on complete wetting of the metal surface; thus, liquid holdup is determined from the packing area and the average film thickness. This approach gives lower values of holdup than those given by the SRP method (see Figure 1).

Experimental Method

The experimental test system at SRP has been described in previous papers.[3,8] Briefly, it comprises a column of 0.43-m inside diameter with standard auxil-

Table 3. SRP-Model Working Equations

(A) Corrugation Geometry and Flow-Related Parameters
characteristic dimension = corrugation side length, s

(B) Preloading Region Pressure Drop

$$\left(\frac{\Delta p}{\Delta z}\right)_{dry} - \left(\frac{\Delta p}{\Delta z}\right)_{preload}[1 - (0.614 + 71.35s)h_l]^5 = 0 \quad (17)$$

dry pressure drop:

$$\left(\frac{\Delta p}{\Delta z}\right)_{dry} = f\left(\frac{\rho_G}{s}\right)\left(\frac{u_{Gs}}{\epsilon \sin \alpha}\right)^2 \quad (18)$$

friction factor:

$$f = A + \frac{B}{\left(\frac{\rho_G u_{Gs} s}{\mu_G}\right)} \quad (19)$$

coefficients of eq 19:

packing	A	B
B1-250	0.194	212.929
B1-250.60	0.100	54.425
B1-400	0.196	133.430
B1-400.60	0.107	33.503
BSH-400	0.166	104.873
BSH-400.60	0.090	127.765

operating liquid holdup:

$$h_l = \left(\frac{4F_t}{s}\right)^{2/3}\left(\frac{3\mu u_{Ls}}{\rho_L \epsilon g_{ef} \sin \alpha}\right)^{1/3} \quad (20)$$

effective gravity:

$$g_e = g\left(\frac{\rho_L - \rho_G}{\rho_L}\right)\left[1 - \frac{\left(\frac{\Delta p}{\Delta z}\right)_{preload}}{\left(\frac{\Delta p}{\Delta z}\right)_{flood}}\right] \quad (21)$$

total holdup correction factor for partial wetting:

$$F_t = \frac{29.12(We_{Ls}\, Fr_{Ls})^{0.15} s^{0.359}}{Re_{Ls}^{0.2} \epsilon^{0.6} (1 - 0.93 \cos \gamma)(\sin \alpha)^{0.3}} \quad (22)$$

in this study: $\cos \gamma = 0.9$

$$Re_{Ls} = (\rho_L u_{Ls} s)/\mu_L \quad (23)$$

$$We_{Ls} = (\rho_L s u_{Ls}^2)/\sigma \quad (24)$$

$$Fr_{Ls} = u_{Ls}^2/(sg) \quad (25)$$

operating liquid film thickness:

$$\delta = (h_t s)/(4F_t) \quad (26)$$

(C) Effective Surface Area

$$a_e = a_p F_t F_{se} \quad (27)$$

surface enhancement factor, in this study: $F_{se} = 0.35$

(D) Mass-Transfer Coefficients

$$k_G = 0.054\left(\frac{\rho_G(u_{Ge} + u_{Le})s}{\mu_G}\right)^{0.8}\left(\frac{\mu_G}{D_G \rho_G}\right)^{0.333}\left(\frac{D_G}{s}\right) \quad (28)$$

$$k_L = 2\sqrt{\frac{D_L u_{Le}}{\pi 0.9 s}} \quad (29)$$

iaries and a capability of operating at pressures in the range of 0.05−4.2 bar. It is completely equipped with a distributed control system, observation windows, and multiple sampling connections and can accommodate a variety of liquid distributor types. For the present tests, the cyclohexane/*n*-heptane mixture was used, with a special trough-type and tubed liquid distributor (provided by Montz; a drawing of the distributor is available), providing 146 pour points/m^2. The tests were run at total reflux, with sequential samples taken to ensure steady-state conditions. The structured packings were placed carefully in the column to a height of 3.0 m, with individual elements rotated 90° with respect to adjacent elements.

Experimental Results

Figure 2 shows representative total reflux performance data for packings with 60° corrugation angles

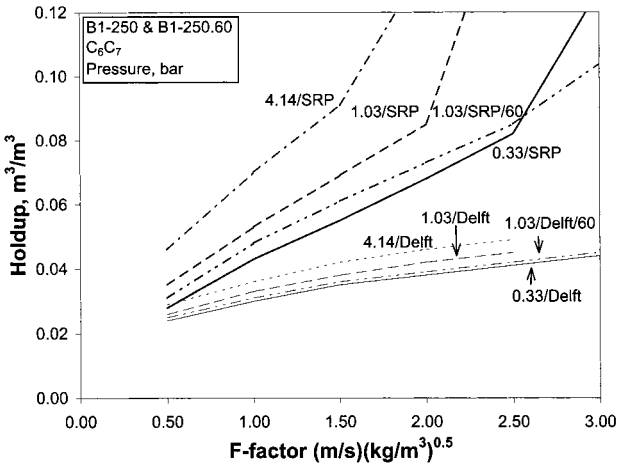

Figure 1. Liquid holdup as predicted by Delft and SRP methods for different operating pressures and corrugation angles.

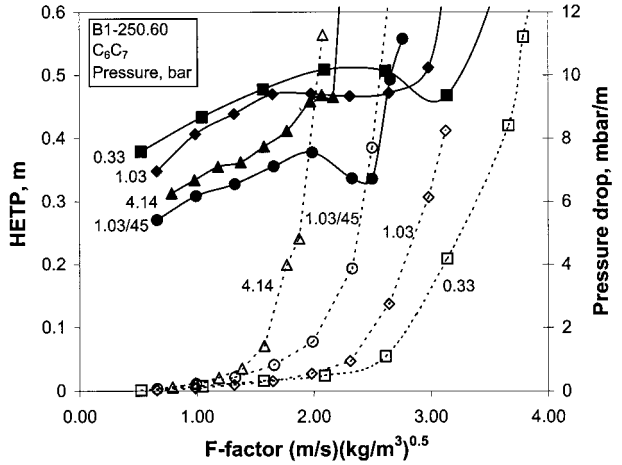

Figure 2. Hydraulic and mass-transfer performance of Montzpak B1-250.60 at total reflux as a function of *F*-factor with operating pressure as the parameter.

(Montz B1-250.60) at three pressures. Atmospheric pressure curves for a "standard" 45° packing (Montz B1-250) have been added to show the effect of corrugation angle on performance. As might be expected, the larger angle provides lower pressure drop and higher capacity, but at the expense of lower efficiency. Throughout this paper, the "standard" B1-250 packing performance data are used for comparison.

Comparison of Model Predictions and Experimental Results

For both models, mass-transfer efficiency is calculated by a two-resistance approach. In the Delft model, the gas-side coefficient accounts for enhancements due to interface roughness and entrance effects. As illustrated in Figure 3 gas-side coefficients from the Delft model are about half those obtained from the SRP model. A compensation for this difference is provided by the effective area used in the two models; as noted above, the SRP model allows for "dry spots" whereas the Delft hydraulic model assumes complete wetting. Thus, the product of the transfer coefficient and the effective area tends to be about the same for the two models. Further support for these different approaches, using controlled experimental work, still is to be done. For the liquid-side coefficient, penetration theory is used for both

Table 4. Delft-Model Working Equations

(A) Corrugation Geometry and Flow-Related Parameters

characteristic packing dimension = hydraulic diameter for gas phase, d_{hG}, as given by eq 11

length of the triangular gas flow channel in a packing element:

$$l_{G,pe} = h_{pe}/(\sin \alpha) \tag{30}$$

V-shaped fraction of the cross section of the triangular gas flow channel occupied by liquid film:

$$\varphi = 2s/(b + 2s) \tag{31}$$

liquid holdup:

$$h_L = \delta a_p \tag{32}$$

mean liquid film thickness:

$$\delta = \left(\frac{3\mu_L u_{Ls}}{\rho_L g a_p \sin \alpha}\right)^{1/3} \tag{33}$$

characteristic Reynolds numbers:

$$Re_{Ge} = (\rho_G u_{Ge} d_{hG})/\mu_G \tag{34}$$

$$Re_{Le} = (\rho_L u_{Le} d_{hL})/\mu_L \tag{35}$$

$$Re_{Grv} = (\rho_{Ge}(u_{Ge} + u_{Le}) d_{hG})/\mu_G \tag{36}$$

hydraulic diameter of the liquid phase:

$$d_{hL} = 4\delta \tag{37}$$

(B) Pressure Drop in Preloading Region

preloading region pressure drop:

$$\Delta p_{preload} = \Delta p_{GL} + \Delta p_{GG} + \Delta p_{DC} = (\zeta_{GL} + \zeta_{GG} + \zeta_{DC})[(\rho_G u_{Ge}^2)/2] \tag{38}$$

overall gas/liquid interaction coefficient:

$$\zeta_{GL} = \varphi \xi_{GL} \frac{h_{pb}}{d_{hG} \sin \alpha} \tag{39}$$

gas/liquid friction factor:

$$\xi_{GL} = \left\{-2 \log\left[\frac{(\delta/d_{hG})}{3.7} - \frac{5.02}{Re_{Grv}} \log\left(\frac{(\delta/d_{hG})}{3.7} + \frac{14.5}{Re_{Grv}}\right)\right]\right\}^{-2} \tag{40}$$

gas/gas interaction coefficient:

$$\zeta_{GG} = (1 - \varphi)\xi_{GG} \frac{h_{pb}}{d_{hG} \sin \alpha} = (1 - \varphi)0.722(\cos \alpha)^{3.14} \frac{h_{pb}}{d_{hG} \sin \alpha} \tag{41}$$

directional change loss coefficient:

$$\zeta_{DC} = \frac{h_{pb}}{h_{pe}}(\xi_{bulk} + \psi \xi_{wall}) \tag{42}$$

with

$$\psi = \frac{2h_{pe}}{\pi d_c^2 \tan \alpha}\left(d_c^2 \frac{h_{pe}^2}{\tan^2 \alpha}\right)^{0.5} + \frac{2}{\pi} \arcsin\left(\frac{h_{pe}}{d_c \tan \alpha}\right) \tag{43}$$

$$\xi_{bulk} = 1.76(\cos \alpha)^{1.63} \tag{44}$$

$$\xi_{wall} = \frac{4092 u_{Ls}^{0.31} + 4715(\cos \alpha)^{0.445}}{Re_{Ge}} + 34.19 u_{Ls}^{0.44} (\cos \alpha)^{0.779} \tag{45}$$

(C) Effective Surface Area

$$a_e = a_p \frac{(1 - \Omega)}{\left(1 + \frac{A}{(u_{Ls})^B}\right)} \qquad A = 0.000\ 002\ 143,\ B = 1.5 \tag{46}$$

fraction of packing surface area occupied by holes Ω: for B1 = 0; for BSH = 0.1.

(D) Mass-Transfer Coefficients

gas-phase mass-transfer coefficient:

$$k_G = \sqrt{k_{G,lam}^2 + k_{G,turb}^2} \tag{47}$$

with

$$k_{G,lam} = \frac{Sh_{G,lam} D_G}{d_{hG}} \tag{48}$$

$$k_{G,turb} = \frac{Sh_{G,turb} D_G}{d_{hG}} \tag{49}$$

and

$$Sh_{G,lam} = 0.664 Sc_G^{1/3} \sqrt{Re_{Grv} \frac{d_{hG}}{l_{G,pe}}} \tag{50}$$

$$Sh_{G,turb} = \frac{Re_{Grv} Sc_G \frac{\xi_{GL}\varphi}{8}}{1 + 12.7\sqrt{\frac{\xi_{GL}\varphi}{8}}(Sc_G^{2/3} - 1)}\left[1 + \left(\frac{d_{hG}}{l_{G,pe}}\right)^{2/3}\right] \tag{51}$$

$$Sc_G = \frac{\mu_G}{\rho_G D_G} \tag{52}$$

liquid-phase mass-transfer coefficient:

$$k_L = 2\sqrt{\frac{D_L u_{Le}}{\pi 0.9 d_{hG}}} \tag{53}$$

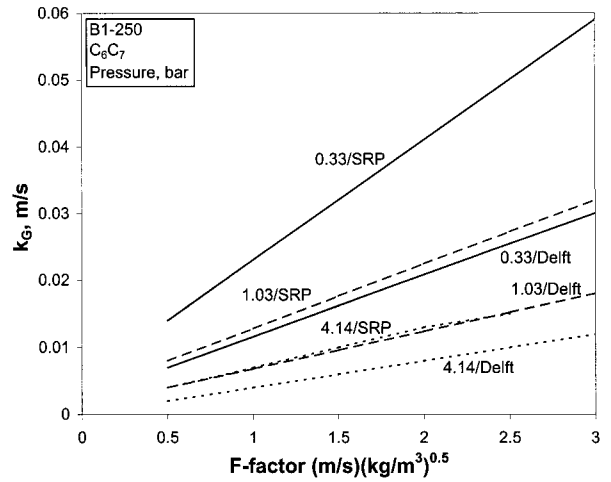

Figure 3. Gas-phase mass-transfer coefficient as predicted by Delft and SRP methods, for B1-250 at different operating pressures.

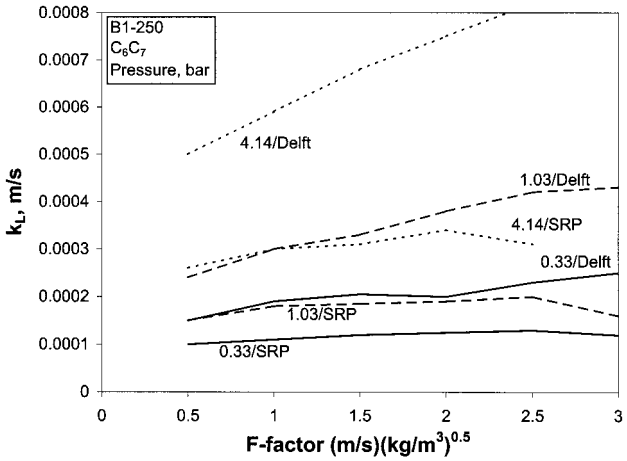

Figure 4. Liquid-phase mass-transfer coefficient as predicted by Delft and SRP methods, for B1-250 at different operating pressures

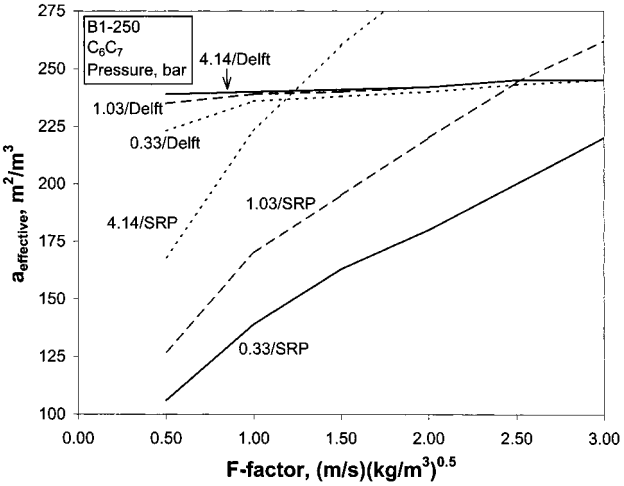

Figure 5. Effective surface area as predicted by Delft and SRP methods for given total reflux conditions.

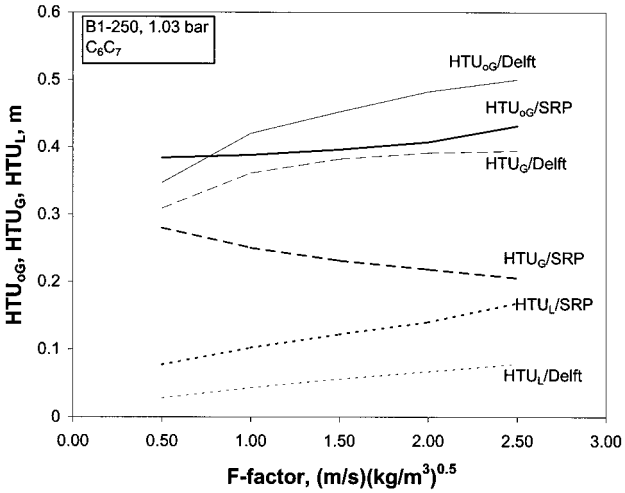

Figure 6. Height of overall, gas-side, and liquid-side transfer units as predicted by Delft and SRP methods.

models; the Delft equivalent channel diameter basis gives somewhat higher values (see Figure 4). At higher loadings, a slight decline of the liquid-side coefficient for the SRP model is attributed to liquid holdup effect, as shown earlier in Figure 1.

For effective surface area, the Delft method is based on a fit of a characteristic exponential curve based on a detailed liquid distribution model,[9] which takes into account observed spreading behavior as a function of liquid load. In the present study use of the Delft model is based on all packings tested having the same wetting behavior as that observed with B1-250 packing. Figure 5 shows that with the SRP approach the wetted surface area increases strongly with both *F*-factor and pressure (i.e., increasing liquid load at total reflux). Above atmospheric pressure the effective area is larger than the specific packing surface, even at *F*-factors slightly below those corresponding to the loading point, where $F_{G,lp,4.14bar} = 1.7$ m/s (kg/m^3)$^{0.5}$. This can be explained in part by the presence of drops and ligaments apart from the metal surface. On the other hand, the Delft method assumes essentially complete wetting well below the loading point and does not account for enhancement of effective surface area, which most probably occurs in the region above the loading point. The strongly increasing trend of effective area given by the SRP model compensates for relatively higher values of the gas-side mass-transfer coefficient and causes the gas-phase transfer unit to decrease with increasing *F*-factor (Figure 6). The trend of the liquid-side coefficient compensates for this and the height of the overall gas-transfer unit increases slightly with increasing *F*-factor. The slope of the curve produced by the Delft method is more pronounced and as a result the same trend carries over to the HETP curves.

Results and Discussion

Pressure drop and mass-transfer efficiency (HETP) as predicted by Delft and SRP methods are reported here as functions of the *F*-factor. Figure 7 shows comparisons of predicted and measured pressure drops of the "standard" B1-250. The predicted load point is determined by the same method for each case, the recently published method of Verschoof et al.[10] In the preloading region, SRP pressure drop values are slightly higher than those of Delft. This relatively higher pressure drop carries through to the loading region because the method for ΔP enhancement is the same. The generally lower preloading pressure drop by the Delft model results largely from a lower predicted liquid holdup. Both methods overpredict the loading point at 4.14 bar.

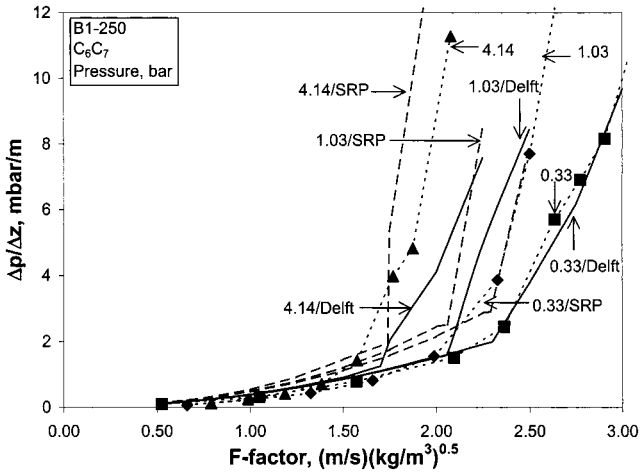

Figure 7. Predicted versus measured pressure drop, with illustration of the operating pressure effect.

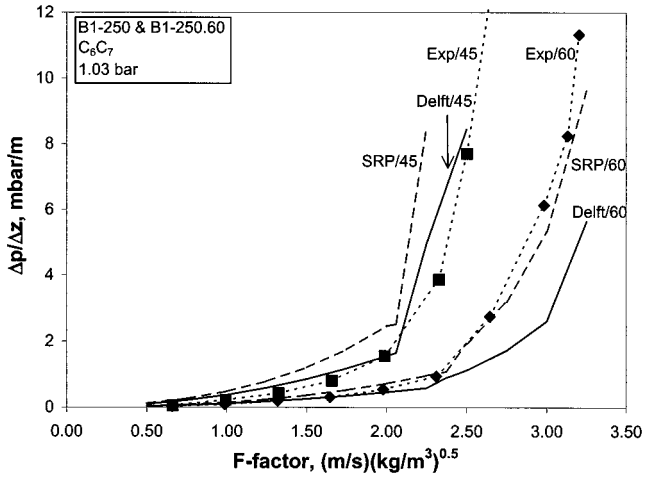

Figure 8. Predicted versus measured pressure drop with illustration of the corrugation angle effect.

Figure 8 shows the effect of corrugation angle on pressure drop of the 250 m^2/m^3 size packings. Both methods predict the load point fairly well. SRP overpredicts the preloading pressure drop of the 45° packing, but predicts well the loading region pressure drop of the 60° packing. For the larger surface area packing (400 m^2/m^3, Figure 9) both methods underpredict the load point of the 45° packing. This deviation is more pronounced for the 45° expanded metal packing (Figure 10). The expanded metal surface has a high percentage of open area which allows the gas to escape to neighboring channels when local liquid overload occurs and vice versa. This ensures a slightly larger capacity compared to that of unperforated sheet metal (B1) packing of the same size.

Predicted and measured HETP curves for the 250 m^2/m^3 size packings are shown in Figures 11 and 12. (In Figure 12, one should note that a 15° increase in corrugation angle has a greater effect on efficiency than what might be expected, recognizing that the surface area of the packing is unchanged. A thorough discussion of the reasons for the angle effect is given elsewhere.[9,10]) The Delft curves follow the trend of measured data points whereas the SRP curves are practically independent of *F*-factor. In Figure 11, the SRP curves follow the observed effect of pressure, whereas the Delft curves do not; in fact, the atmospheric pressure curve lies above that for vacuum conditions. This might be corrected by

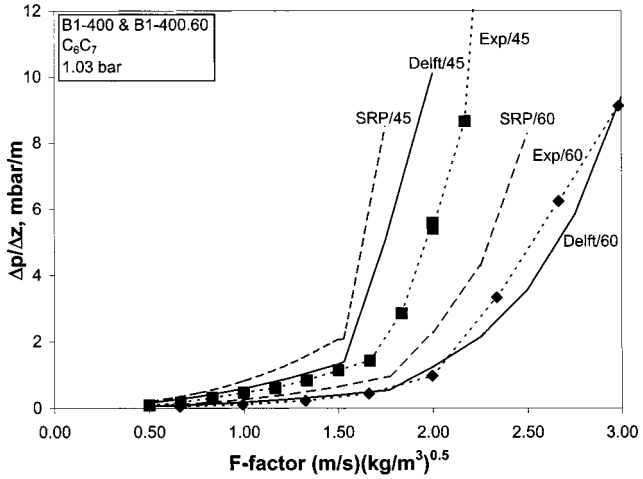

Figure 9. Predicted versus measured pressure drop of large surface area packing, with illustration of the corrugation angle effect.

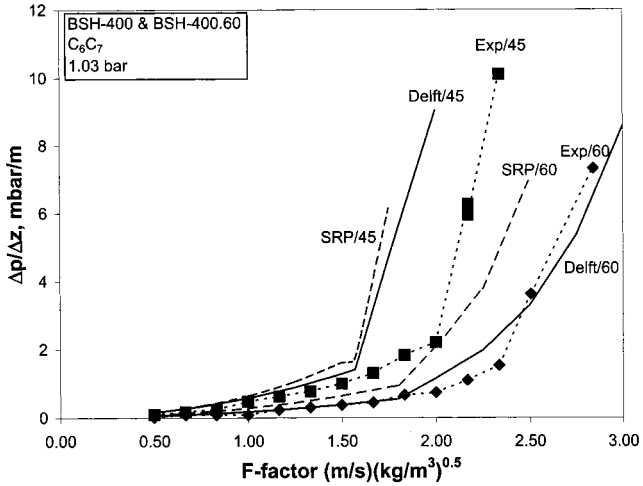

Figure 10. Predicted versus measured pressure drop of large surface area packing made of expanded metal, with illustration of the corrugation angle effect.

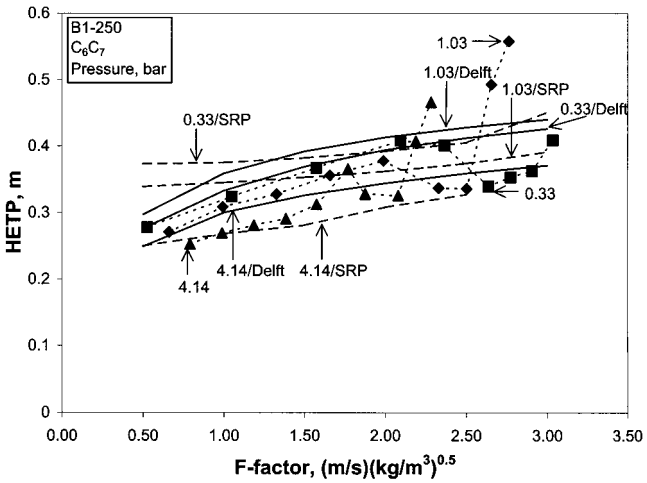

Figure 11. Predicted versus measured HETP, with illustrations of the operating pressure effect.

anticipating a somewhat lower effective area than that predicted by the empirical correlation based on liquid-spreading experiments at atmospheric conditions. At vacuum conditions, the predicted curve fits very well with the measured one.

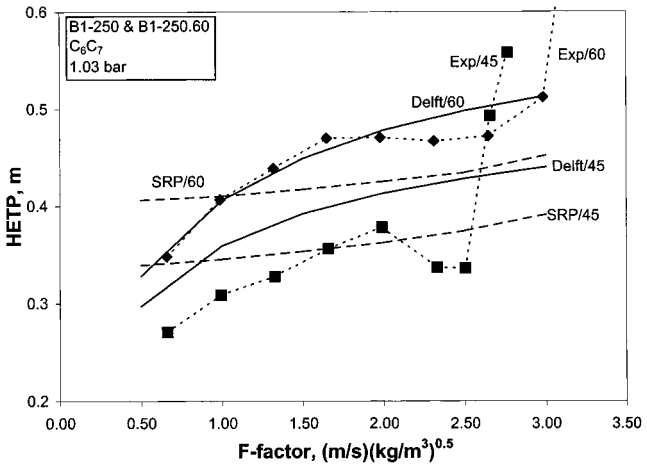

Figure 12. Predicted versus measured HETP, with illustration of the corrugation angle effect.

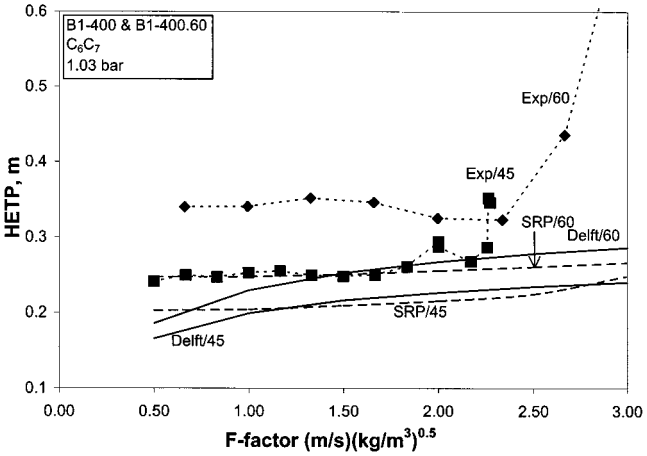

Figure 13. Predicted versus measured HETP of a large surface area packing, with illustration of the corrugation angle effect.

With regard to the corrugation angle effect on HETP (Figure 12), the Delft method gives a very good fit for the 60° packing whereas the SRP method gives a better fit at 45°. However, for both methods the calculated difference in HETP values between 45° and 60° angles is smaller than that observed. This indicates that some additional phenomenon, probably related to the effective flow angle and its effect on a wetted surface, plays a more pronounced role here than anticipated in model equations.

For packings with larger surface areas and particularly for the BSH type, neither method anticipates the large effect of angle on HETP as shown in Figures 13 and 14. One should note that for the BSH packing the less pronounced deviation of the Delft method is because it employs an additional factor for surface area reduction, which corresponds quantitatively to the fraction of area occupied by holes. As suggested in a recent publication,[11] a closer approach to measured curves might be obtained by taking into account a larger loss of surface area than the 10% represented by holes. Organic liquids make more use of the holes to pass through the sheet, and liquid-spreading tests indicate that organic liquids can also penetrate to some extent the small apertures in the expanded metal surface. This affects liquid distribution adversely and results in reduced holdup. In general, it appears that packings with large areas experience a relatively larger loss of active area than the more common size packings.

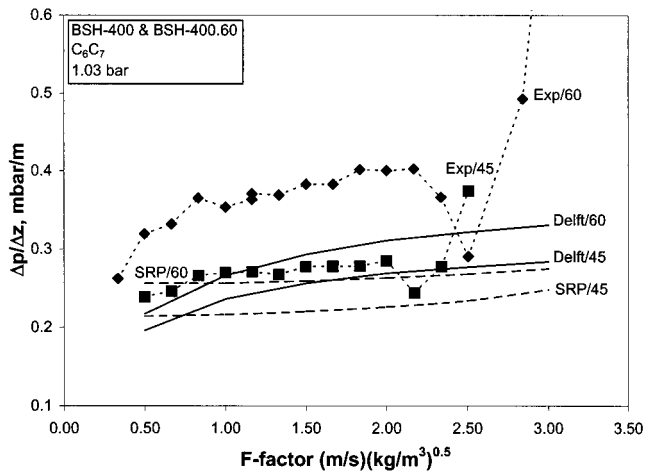

Figure 14. Predicted versus measured HETP of a large surface area packing made of expanded metal, with illustration of the corrugation angle effect.

Table 5. SRP and Delft Model Refinements Considered in This Study

Effective Surface Area

Onda et al.[13] correlation with specific surface area (original), corrugation side or hydraulic diameter for gas flow as characteristic length dimension:

$$a_e = a_p\{1 - \exp[-1.45(0.075/\sigma)^{0.75}Re_{Ls}^{0.1}Fr_{Ls}^{-0.05}We_{Ls}^{0.2}]\}$$

Liquid Holdup and Liquid-Phase Mass-Transfer Coefficient

Shetty and Cerro[15] correlations:

$$h_L = 6.096Re_{Ls}^{1/3}Ga_L^{-1.3}$$

and

$$k_L = 0.4185\,((\sin\alpha)/l_{ratio})^{1/2}(Re_{Ls}^{1/3}Ga_L^{1/6}Sc_L^{1/2})(D_L/b)$$

with

$$l_{ratio} = 3.617 - 0.122\,99\alpha + 0.001976\alpha^2 - 0.000\,011\,167\alpha^3$$

(α in radians)

$$Re_{Ls} = (\rho_L u_{Ls} b)/\mu_L$$

$$Ga_{Ls} = (gb^3\rho_L^2)/\mu_L^2$$

and

$$Sc_L = \mu_L/(\rho_L D_L)$$

effective liquid flow angle

Spekuljak and Billet[16] correlation:

$$\alpha_{L,e} = a\tan\left[\frac{\cos(90-\alpha)}{\sin(90-\alpha)\cos\left[a\tan\left(\frac{b}{2h}\right)\right]}\right]$$

Both methods were designed to model mass-transfer efficiency in the preloading region, which implies a conservative approach when extended into the loading region. Furthermore, the physical situation in the loading region is very complex and depends strongly on surface design and corrugation angle. Our present understanding of phenomena in the loading region is probably not sufficient to justify more sophisticated attempts at modeling.

Model Improvement Considerations

Confronted with deficiencies of the methods that are discussed above, we conclude that liquid flow-related parameters are probably not represented adequately. Table 5 summarizes correlations available in the literature which do not require any additional packing-specific coefficient and therefore could be incorporated into our models.

A more accurate method for predicting interfacial area is a prerequisite if one wishes to arrive at a more reliable predictive model for mass-transfer efficiency. And this may have to await further development of

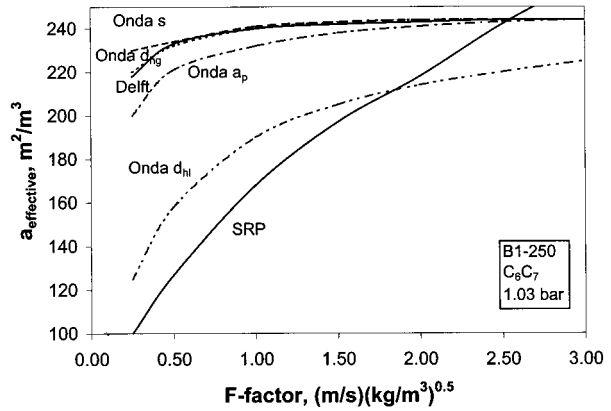

Figure 15. Effective surface area as predicted for given total reflux conditions by Onda et al.[11] correlation with specific surface area, corrugation side, hydraulic diameter of gas flow, and hydraulic diameter of liquid flow as characteristic length dimension.

noninvasive, experimental imaging techniques, such as X-ray tomography.[12] As illustrated in Figure 15 , on one hand, for the SRP model and its hydraulic diameter for liquid flow, the well-known and widely accepted correlation of Onda et al.,[13] developed originally for first-generation random packings, produces reasonable correspondence. On the other hand, for the Delft model and its characteristic diameter, the Onda correlation produces nearly the same values of interfacial area as the original empirical correlation. (For the plot, hydraulic diameter for the gas is used as the characteristic dimension.)

We have also evaluated the approach suggested by Hanley et al.,[14] which assumes a reduced interfacial area at low *F*-factors and above the loading point. The preloading part of this correlation, with absolute effective surface area values between those predicted by the original Delft correlation or the adapted Onda correlation and the SRP correlation, improves the accuracy of SRP predictions of HETP. However, the loading region part forces the HETP curve to a correspondingly sharp deterioration, which occurs at conditions closer to the load point than to the flood point. Certainly, a more complex form of interfacial area function is required if one wishes to simulate pronounced performance enhancement, as observed with 45° Montz packings. Unfortunately, this would require even more adjustable parameters than those used by Hanley et al.[14]

A less obvious area for improvement would be the development of theoretical correlations for liquid film flow based on design parameters such as liquid holdup and mass-transfer coefficients. A fundamentally sound basis for structured packings has been provided recently by Shetty and Cerro.[15] As can be seen from Table 5, their correlations for holdup and the liquid-side mass-transfer coefficient include the Galileo number, with the corrugation base length as the characteristic dimension, to account explicitly for liquid film thickness. Implementing their results into the present methods has not resulted in improvements, however. Also, knowing from experience that in most cases the liquid flows down through the packing at an angle larger than the corrugation angle, which implies a certain decrease in liquid holdup, we have introduced into our models the effective liquid flow angle, calculated according to a theoretically based expression by Spekuljak and Billet[16] (see Table 5), but this has resulted for both models in only minor improvements, mainly at higher liquid loads.

For the gas mass-transfer coefficient, the Delft correlation is directly related to gas−liquid friction and takes into account the enhancement due to entrance effects. Its strength is also in the triangular cross-section based hydraulic diameter which allows for the effect of the change in the corrugation height-to-base ratio. The SRP method uses a wetted-wall model as a point of departure. The surface enhancement factor, which varies within a rather limited range, is an adjustable parameter. The use of packing type and size-specific constants may make the SRP method less amenable to further generalization.

Concluding Remarks

A consistent set of total reflux distillation test data has been used to validate the SRP and Delft models for predicting hydraulic and mass-transfer performance of structured packings. The tests have involved a set of Montz packings. In general, the SRP method overpredicts pressure drop and underpredicts mass-transfer efficiency, both usually considered conservative for design. The Delft method predicts slightly larger HETP values for vacuum conditions than for atmospheric conditions, but not at the expense of overall accuracy, however. Both methods are too optimistic for packings with larger specific surface areas and generally predict too small a difference in mass transfer resulting from the corrugation angle effect. The rather strong effect of this angle on pressure drop is predicted fairly well by both methods.

Improved modeling of the effective interfacial area is a key requirement for increasing the reliability and overall accuracy of both methods. A possibility might be adaptation of the Onda approach to structured packing geometry. In that case, no packing-specific coefficients would be needed.

Acknowledgment

The authors wish to thank Julius Montz GmbH for providing a uniform set of packings and for permitting the test results to be shared with the general public. They also acknowledge funding by the Separations Research Program, to enable the operation of the research equipment, and the work of Mr. Jacinto Lopez-Toledo in preparing the figures.

Nomenclature

a_p = specific surface area of packing, m^2/m^3
a_e = effective surface area, m^2/m^3
b = corrugation base length, m
D_G = gas-phase diffusion coefficient, m^2/s
D_L = liquid-phase diffusion coefficient, m^2/s
d_c = column diameter, m
d_{hG} = hydraulic diameter for the gas phase, m
$F_{G,lp}$ = loading point gas load factor, m/s $(kg/m^3)^{0.5}$
F_{load} = loading effect factor
F_t = partial wetting correction factor
F_{se} = surface enhancement factor
Fr_{Ls} = Froude number for liquid
g = gravity acceleration, m/s^2
HETP = height equivalent to a theoretical plate, m
HTU_G = height of a gas-phase transfer unit, m
HTU_L = height of a liquid-phase transfer unit, m
HTU_{Go}= height of an overall gas-phase-related transfer unit, m
h = corrugation height, m

h_L = operating liquid holdup
h_{pb} = height of the packed bed, m
h_{pe} = height of the packing element, m
k_G = gas-phase mass-transfer coefficient, m/s
k_L = liquid-phase mass-transfer coefficient, m/s
L = molar flow rate of liquid, kmol/s
$l_{G,pe}$ = length of gas flow channel in a packing element, m
m = slope of the equilibrium line
n_{pe} = number of packing elements (layers) in a bed
Re_{Ge} = effective gas-phase Reynolds number
Re_{Grv} = relative velocity Reynolds number
Sc_G = Schmidt number for gas
s = corrugation side length, m
u_{Ge} = effective gas velocity, m/s
$u_{Ge,lp}$ = effective loading point gas velocity, m/s
u_{Gs} = superficial gas velocity, m/s
u_{Le} = effective liquid velocity, m/s
u_{Ls} = superficial liquid velocity, m/s
V = molar flow rate of vapor, kmol/s
We_L = Weber number for the liquid

Greek Letters

α = corrugation inclination angle, deg
α_{lk} = relative volatility of the light component
γ = contact angle between solid and liquid film, deg
δ = liquid film thickness, m
ζ_{DC} = overall coefficient for direction change losses
ζ_{GG} = overall coefficient for gas−gas friction losses
ζ_{GL} = overall coefficient for gas−liquid friction losses
ϵ = packing porosity, m^3 of voids/m^3 of bed
$\lambda = m/(L/V)$ = stripping factor
μ_G = viscosity of gas, Pa s
μ_L = viscosity of liquid, Pa s
ξ_{bulk} = direction change factor for bulk zone
ξ_{GG} = gas−gas friction factor
ξ_{GL} = gas−liquid friction factor
ξ_{wall} = direction change factor for wall zone
ρ_G = density of gas, kg/m^3
ρ_L = density of liquid, kg/m^3
φ = fraction of the triangular flow channel occupied by liquid
Ψ = fraction of gas flow channels ending at column walls
Ω = fraction of packing surface area occupied by holes

Subscripts

e = effective
G = gas or vapor
lam = laminar flow
L = liquid
s = superficial
turb = turbulent flow

Literature Cited

(1) Bravo, J. L.; Rocha, J. A.; Fair, J. R. Mass Transfer in Gauze Packings. *Hydrocarbon Process.* **1985**, *64* (1), 91.

(2) Bravo, J. L.; Rocha, J. A.; Fair, J. R. A Comprehensive Model for the Performance of Columns Containing Structured Packings. *Inst. Chem. Eng. Symp. Ser.* **1992**, *128*, A489.

(3) Rocha, J. A.; Bravo, J. L.; Fair, J. R. Distillation Columns Containing Structured Packings: A Comprehensive Model for Their Performance. 1. Hydraulic Models. *Ind. Eng. Chem. Res.* **1993**, *32*, 641. 2. Mass Transfer Model. *Ind. Eng. Chem. Res.* **1996**, *35*, 1660.

(4) Olujic, Z. Development of a Complete Simulation Model for Predicting the Hydraulic and Separation Performance of Distillation Columns Equipped with Structured Packings. *Chem. Biochem. Eng. Q.* **1997**, *11*, 31.

(5) Olujic, Z. Effect of Column Diameter on Pressure Drop of a Corrugated Sheet Structured Packing. *Trans. Inst. Chem. Eng.* **1999**, *77* (Part A), 505.

(6) Olujic, Z.; Kamerbeek, A. B.; de Graauw, J. A Corrugation Geometry Based Model for Efficiency of Structured Distillation Packing, *Chem. Eng. Process.* **1999**, *38*, 683.

(7) Gualito, J. J.; Cerino, F. J.; Cardenas, J. C.; Rocha, J. A. Design Method for Distillation Columns Filled with Metallic, Ceramic, or Plastic Structured Packings. *Ind. Eng. Chem. Res.* **1997**, *36*, 1747.

(8) Fair, J. R.; Bravo, J. L. Distillation Columns Containing Structured Packing. *Chem. Eng. Prog.* **1990**, *86* (1), 19.

(9) Olujic, Z.; Roelofse, A.; Stoter, F.; de Graauw, J. LDESP: A Simulation and Optimisation Environment for Structured Packings. *Inst. Chem. Eng. Symp. Ser.* **1997**, *142*, 949.

(10) Verschoof, H.-J.; Olujic, Z.; Fair, J. R. A General Correlation for Predicting the Loading Point of Corrugated Sheet Structured Packings. *Ind. Eng. Chem. Res.* **1999**, *38*, 3663.

(11) Seibert, A. F.; Fair, J. R.; Olujic, Z. Influence of Corrugation Geometry on the Performance of Structured Packings: An Experimental Study. AIChE Spring National Meeting, Houston, March 14−18, 1999; *Topical Conference Preprints—Distillation: Horizons for the New Millennium*; AIChE: New York, 1999; p 269.

(12) Marchot, P.; Toye, D.; Crine, M.; Pelsser, A.-M.; L'Homme, G. Investigation of Liquid Maldistribution in Packed Columns by X-ray Tomography. *Trans. Inst. Chem. Eng.* **1999**, *77* (Part A), 511.

(13) Onda, K.; Takeuchi, H.; Okumoto, Y. Mass Transfer Coefficients Between Gas and Liquid Phases in Packed Columns, *J. Chem. Eng. Jpn.* **1968**, *1*, 56. (Originally published in *Kagaku Kogaku* **1967**, *31*, 126.)

(14) Hanley, B.; Dunbobbin, B.; Bennett, D. A Unified Model for Countercurrent Vapor-Liquid Packed Columns. 2. Equations for Mass Transfer Coefficients, Mass Transfer Area and the HETP. *Ind. Eng. Chem. Res.* **1994**, *33*, 1222.

(15) Shetty, S.; Cerro, R. L. Fundamental Liquid Flow Correlations for the Computation of Design Parameters of Ordered Packings. *Ind. Eng. Chem. Res.* **1996**, *36*, 771.

(16) Spekuljak, Z.; Billet, R. Mass Transfer in Regular Packing. *Rev. Latinoam. Transferencia Calor. Mater.* **1987**, *11*, 63.

Received for review December 21, 1999
Revised manuscript received February 23, 2000
Accepted March 21, 2000

IE990910T